Electronic Supplementary Material (ESI) for Journal of Materials Chemistry A.

Rigidity of Organic Interlayer on Affecting the Nonradiative Recombination and Exciton Dissociation in Hybrid Dion−Jacobson 2D Lead Iodide Perovskites

Kexuan Sun[a,b], Yuanyuan Meng[a*], Ruikun Cao[a] , Yumin Ren[d], Yuhong Mao[c], Ruijia Tian[a], Yaohua Wang[a], , Xujie Lü[c], Chang Liu[a,b]*, Ziyi Ge[a,b]*

[a]Zhejiang Provincial Engineering Research Center of Energy Optoelectronic Materials and Devices, Ningbo Institute of Materials Technology & Engineering, Chinese Academy of Sciences, Ningbo 315201, China

[b]Center of Materials Science and Optoelectronics Engineering University of Chinese Academy of Sciences, Beijing 100049, China

[c]Center for High Pressure Science and Technology Advanced Research (HPSTAR), Shanghai 201203, China

[d]School of Chemistry, Xi'an Jiaotong University, Xi'an, Shaanxi Province, 710049, China

*Corresponding authors E-mail: mengyuanyuan@nimte.ac.cn; liuchang1@nimte.ac.cn; geziyi@nimte.ac.cn;

Experimental method

1. Materials

3-(Aminomethyl)piperidine (3AMP, 98%), N,N-dimethyl formamide (DMF, 99.8%), Dimethyl sulfoxide (DMSO, 99.7%), and chlorobenzene (CB, 99.9%) were purchased from Beijing J&K Scientific Ltd. 4-(Aminomethyl)piperidine (4AMP, 98%), Lead oxide(PbO,99.9%) were purchased from Shanghai Aladdin Biochemical Technology Co., Ltd. Hydriodic (HI, 57 wt. %), Hypophoaphoeous acid (H_3PO_2, 50 wt. % in H_2O) Shanghai Macklin Biochemical Technology Co. bathocuproine (BCP,99.9%), Lead(II) iodide (PbI_2, 99.99%) and Formamidine Iodide (FAI, 99.9%), and the FTO/Glass substrate were purchased from Advanced Election Technology CO., Ltd. [6,6]-phenyl-C61-butyric acid methyl ester ($PC_{61}BM$, 99%) from Lumtec. [2-(3,6-Dimethoxy-9H-carbazol-9-yl)ethyl]phosphonic acid (MeO-2PACz, 98.0%) from TCI.All these commercially available materials were used directly as received without any further purification

2. Precursor Solution Preparation

To obtain the perovskite precursor solution, the first step is to synthesize (3AMP)$FAPb_2I_7$ and (4AMP)$FAPb_2I_7$ crystals, Dissolve 3mmol PbO in 6ml of hydroiodic acid and 1ml of hypophosphoric acid solution at 130 °C for ten minutes until the solution turned clear bright yellow. Add 2 mmol of Formamidinium iodide (FAI) directly to the above solution under heating. Add 0.5mL of hydroiodic acid to 0.5mmol of 3AMP at 130 °C. Add the 3AMP, hypophosphoric acid mixed solution to the previous solution and continue heating at 130 °C for 5 minutes. Reduce the heated solution to 120 °C at a rate of 0.5 °C per hour and hold for 1 hour. After the crystals precipitate, lower it to room temperature at a rate of 1 °C per hour. Dissolve the crystal in DMF solution after drying. (4AMP)$FAPb_2I_7$ uses the same method and concentration ratio. The experimental ratios (3AMP:MAI:PbO and 4AMP:MAI:PbO) (in mmol) of the (3AMP)$(FA)_4Pb_5I_{16}$ are 0.12:2:2 and (4AMP)$(FA)_4Pb_5I_{16}$ are 0.12:2:2.

3. Devices Fabrication

The inverted PSCs architecture is FTO/MeO-2PACz/perovskite/$PC_{61}BM$/BCP/Ag. All devices were prepared on cleaned and UV treated FTO substrates. 0.6 mg MeO-2PACz was dissolved in 2 mL ethanol. Then, an ultrathin layer of MeO-2PACz was deposited by spin-coating at 3000 rpm for 30s, then annealed at 120 °C for 10 min. The perovskite layer was spin-coated in one-step procedure at 5000 rpm for 30 s, and 200 μL of CB ether was dropped onto the substrate in the last 20 s, then the

films were annealed at 150 °C for 20 min. Afterward, an electron transport layer of $PC_{61}BM$ (20 mg mL^{-1} in CB) and BCP (0.5 mg mL^{-1} saturated solution in IPA) were spin-coated at 3000 rpm for 30 s and 4000 rpm for 30 s, respectively. Finally, a 100 nm thick Ag electrode was deposited by thermal evaporation. The active area of 0.04 cm^2 was defined by a metal mask.

4. Film Characterization

Depth resolved GIXRD were characterized using a Rigaku SmartLab five-axis X-ray diffractometer at 45 kV and 200 mA, equipped with Cu Kα radiation (λ = 1.54050 Å), parallel beam optics and a secondary graphite monochromator. Grazing incident wide-angle X-ray scattering (GIWAXS) measurements were performed by the XEUSS SAXS/WAXS equipment, at an incident angle of 0.5º. For the PL measurement, a 435nm continuous laser was used for excitation. Time-resolved fluorescence was analyzed using the Edinburgh instrument, while FLS 980 fluorescence spectrometer was deployed for TRPL decay excitation measurement. Symmetrical diamond anvil cells, using Type II-a ultralow-fluorescence diamonds with a culet size of 500μm, were employed to create a high-pressure environment. To form the high-pressure sample chamber, a preindented T301 gasket with a thickness of approximately 50μm and a 300μm diameter hole in its center was laser-drilled. Single crystals were exfoliated into thin flakes and transferred onto the diamond culets. The ruby fluorescence method was used to determine the pressure, with mineral oil serving as the pressure transmitting medium. For the absorption measurements, a Xe lamp (EQ-99X-FC-S) was chosen as the white light source. The C-2-V spectra were measured using the Chenhua CHI760E electrochemical workstation. Femtosecond transient absorption spectroscopy were measured by SOL-F-K-HP-T in 400 nm.

5. Device Characterization

Testing current density versus voltage (J-V) curves, stabilized power output (SPO), and steady-state current density curves under AM 1.5G, measuring the dependence of VOC/JSC on light intensity curves by varying the light intensity, and characterizing the conductivity and the space-charge-limited current analysis under dark conditions were all done using the Newport oriel sol3A 450 W solar simulator. Device EQE spectra were measured using the solar cell quantum efficiency measurement equipment (Elli Technology Taiwan). The impedance spectroscopy (IS) and Mott-Schottky curves were calculated using the Chenhua CHI760E

electrochemical workstation. The 1240A Impedance Analyzer captured the curves of capacitance versus frequency (C-F). A REPS measurement tool (Enlitech) was used to apply external voltage/current sources via the PSCs in order to measure the EQEEL. The operational stability test of the monolithic perovskite/silicon tandem solar cell was carried out at the maximum power point (MPP) in N_2 environment under AM1.5 xenon lamp illumination (100 mW cm^{-2}, without UV–filter).

6. Theoretical Calculation

The DFT calculations in this research are performed using the Vienna ab initio simulation software (VASP). To simulate electron exchange-related interactions, the Perdew–Burke–Ernzerhof (PBE) functional is utilized, and the projection enhanced wave (PAW) approach is used for electron–ion–nucleus interactions. In order to handle van der Waals interactions in perovskites, we employ the Grimme DFT-D3 approach with Becke-Johnson damping. Geometry optimization is carried out with the Γ-centered 3×3×2 Monkhorst−Pack k-point mesh and the 400eV plane wave energy cutoff. The geometric structure is regarded as convergent when the energy difference between all ions is smaller than -10^{-6}eV. [1–4]

7. Calculation Methods

1) Trap density of states (tDOS) measurement

The tDOS can be deduced from eq.1 and eq.2

$$tDOS = -\frac{V_{bi}\ \omega\ dC}{qWkTd\omega}\#(1)$$

$$E_{\omega} = kTln\left(\frac{\beta T^2}{\omega}\right)\#(2)$$

where V_{bi} is the built-in potential, q is the elementary charge, W is the depletion width derived from Mott-Schottky curves (Figure 5g), T is the variable temperature, k is the Boltzmann constant, ω is the frequency, C is the capacitance, and β is the intercept of the Arrhenius plots derived from Figure 5d. Finally, figure 4b can be obtained by plotting $tDOS$ vs. E_{ω}

2) Carrier recombination lifetimes calculation[7]

The carrier recombination lifetimes can be derived from the time-resolved photoluminescence (TRPL) by a bi-exponential fitting as shown in eq.3

$$Y = A_1 e^{\left(-\frac{t}{\tau_1}\right)} + A_2 e^{\left(-\frac{t}{\tau_2}\right)} \#(3)$$

where τ is the carrier recombination lifetime, τ_1 and τ_2 are the decay components of the trap-assisted and radiative recombination process respectively. The carrier recombination lifetime can be calculated by eq.4

$$\tau = \frac{A_1\tau_1^2 + A_2\tau_2^2}{A_1\tau_1 + A_2\tau_2} \#(4)$$

3) Analyzation of Mott-Schottky curves

Nd can be calculated by eq.5

$$\frac{dC^{-2}}{dV} = \frac{2}{A^2 q\varepsilon\varepsilon_0 N_d} \#(5)$$

where $\frac{dC^{-2}}{dV}$ is the slope of the fitting line, q is the electron charge, A is the area of PSC, ε_0 and ε are the vacuum permittivity and relative dielectric constant of perovskite.

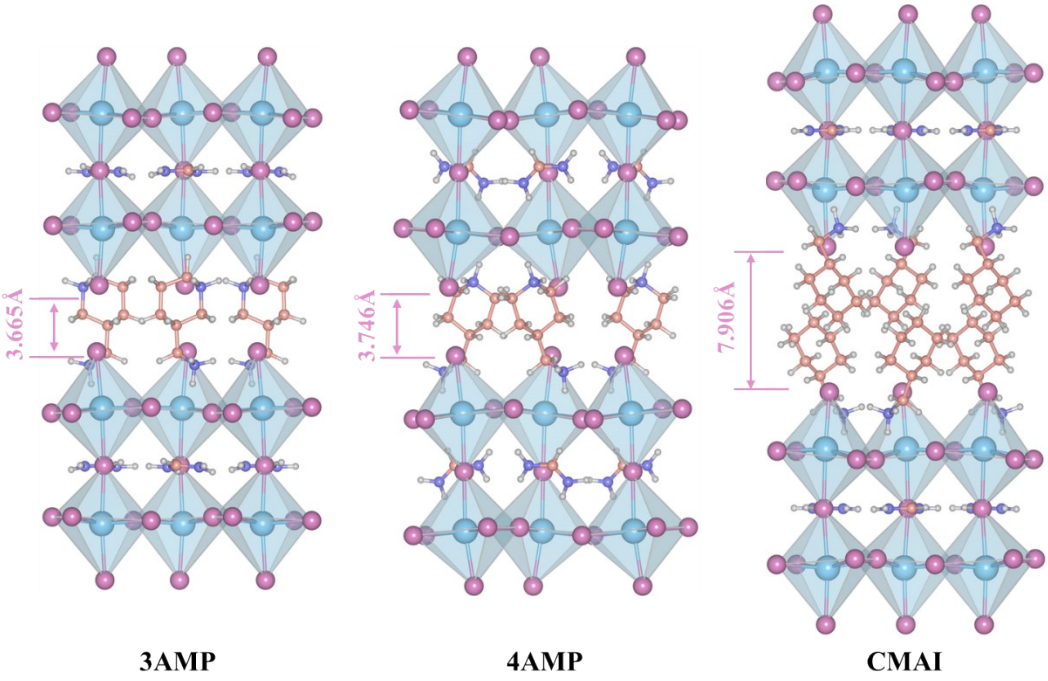

Figure S1.

Models of $(3AMP)(FA)Pb_2I_7$, $(3AMP)(FA)Pb_2I_7$, and $(CMA)_2(FA)Pb_2I_7$ after structural optimization at 1GPa

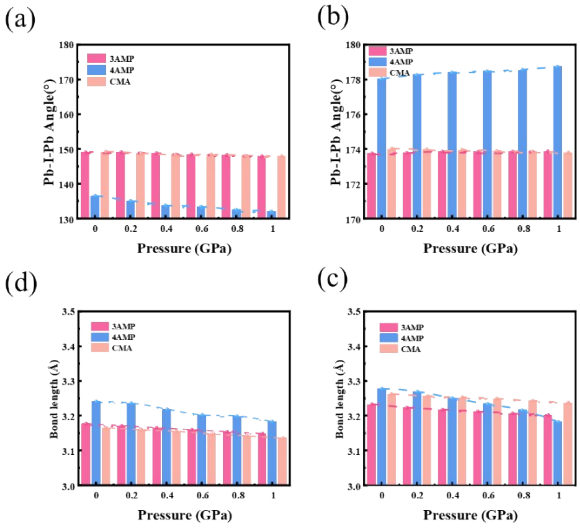

Figure S2.

(a) Changes in Pb-I-Pb between octahedral angles in the parallel direction under pressure

(b) Changes in I-Pb-I between octahedral angles in the vertical direction under pressure

(c) Change in Pb-I bond length under pressure in the parallel direction

(d) Change in Pb-I bond length under pressure in the vertical direction

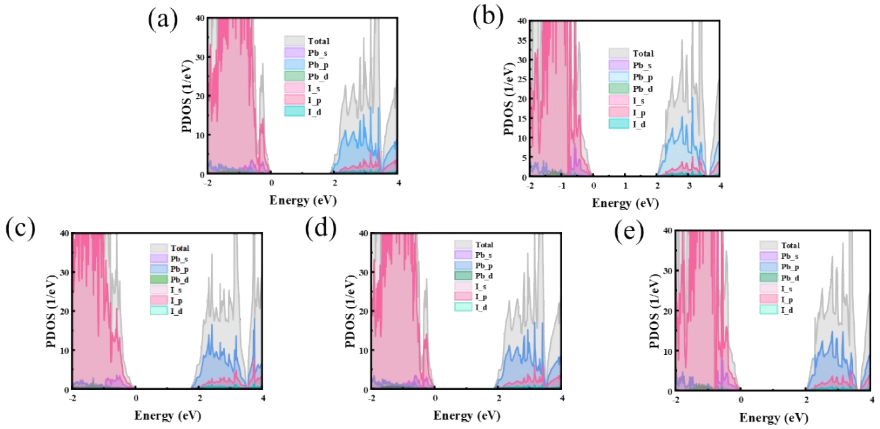

Figure S3

(a) The density of states (DOS) of (4AMP)$FAPb_2I_7$ at 0GPa

(b) The density of states (DOS) of $(CMA)_2FaPb_2I_7$ at 0GPa

(c) The density of states (DOS) of (3AMP)$FAPb_2I_7$ at 1GPa

(d) The density of states (DOS) of (4AMP)$FAPb_2I_7$ at 1GPa

(e) The density of states (DOS) of $(CMA)_2FaPb_2I_7$ at 1GPa

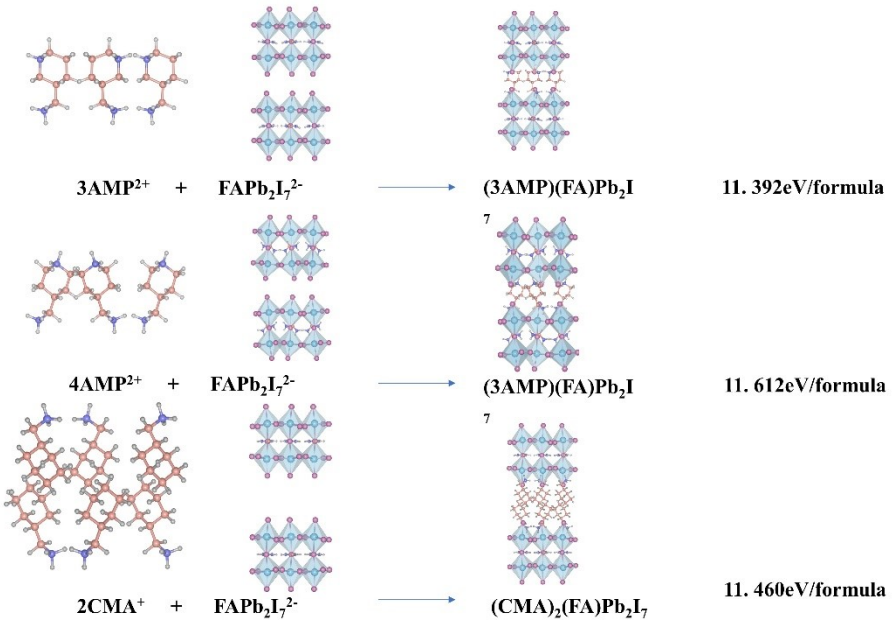

Figure S4.

H-bonding interaction energies between cations and inorganic layers, calculated by VASP. The structures of $3AMP^{2+}$, $4AMP^{2+}$, $2CMA^{2+}$ and $(PbI4)^{2-}$ for the calculation are directly obtained from the (3AMP)$FAPb_2I_7$, (4AMP)$FAPb_2I_7$ and $(CMA)_2FaPb_2I_7$ single crystals by eliminating inorganic or organic parts.

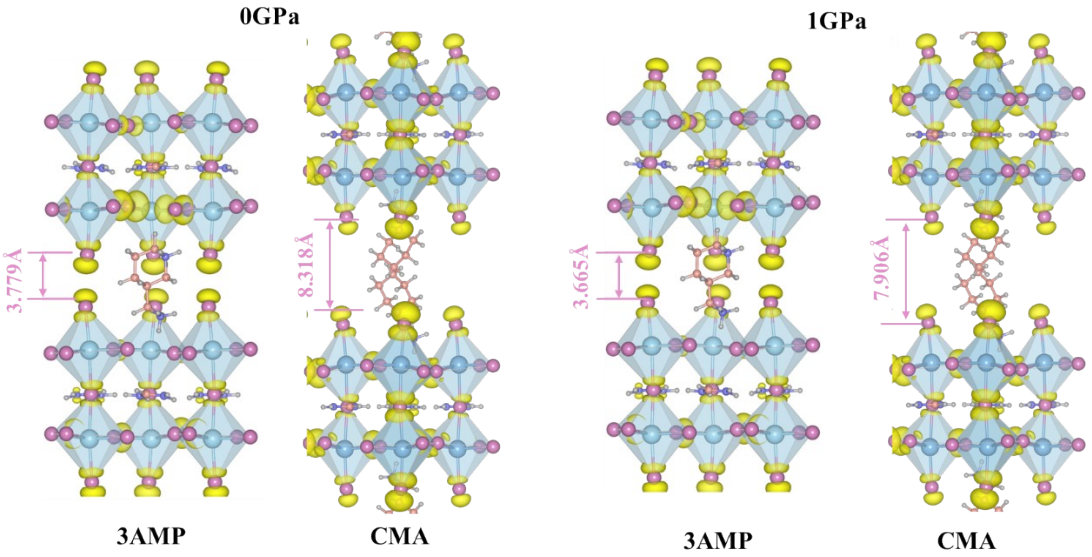

Figure S5.

Charge density distribution of DJ((3AMP)FAPb_2I_7) and RP(($(CMA)_2FaPb_2I_7$) structures at 0GPa and 1GPa

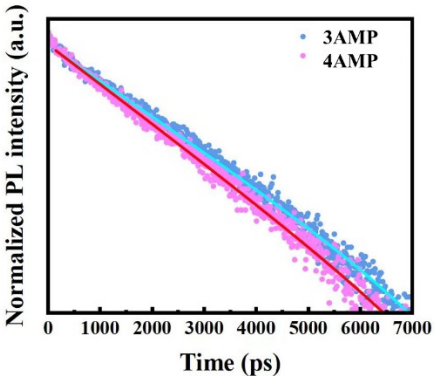

Figure S6.

Time-resolved photoluminescence (TRPL) spectra of (3AMP)(FA)Pb_2I_7 and (4AMP)(FA)Pb_2I_7 perovskite film.

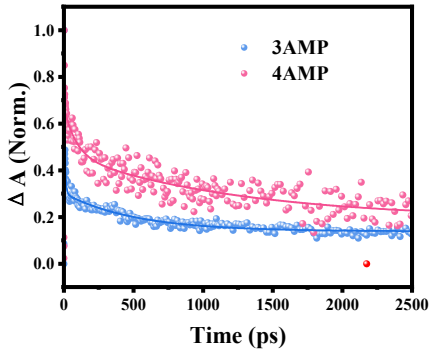

Figure S7.

Decay kinetics at 570 nm of (3AMP)(FA)Pb_2I_7 perovskite film and 530 nm of (4AMP)(FA)Pb_2I_7 perovskite film.

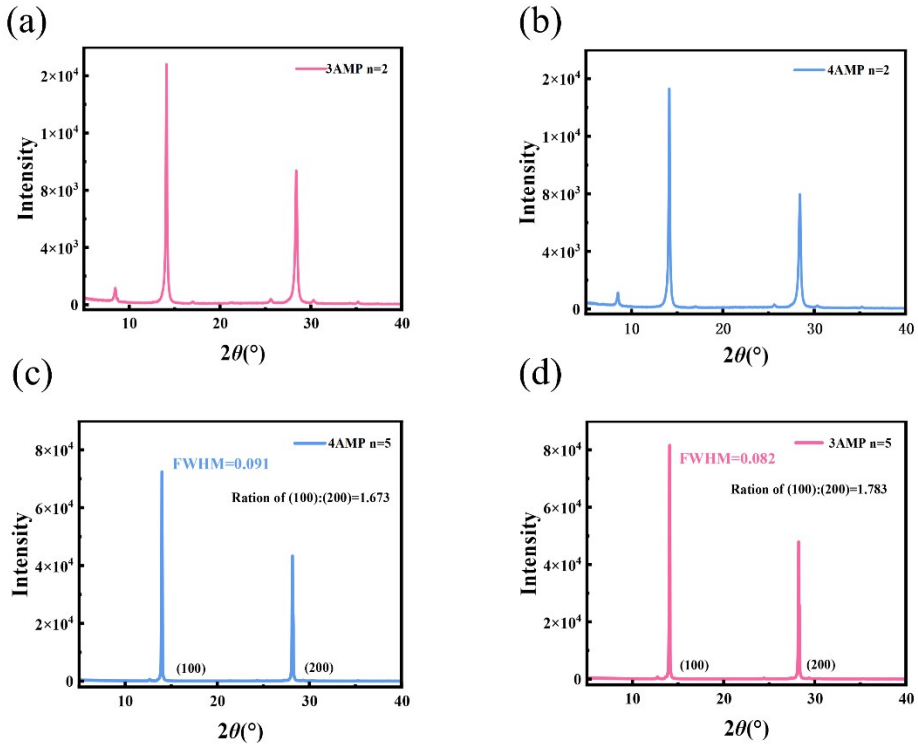

Figure S8.

a) XRD for the (3AMP)$FAPb_2I_7$. b) XRD for the (4AMP)$FAPb_2I_7$.

c) XRD for the (3AMP)$FA4Pb_5I_{16}$ (3AMP-based). d) XRD for the (4AMP)$FA4Pb_5I_{16}$ (4AMP-based).

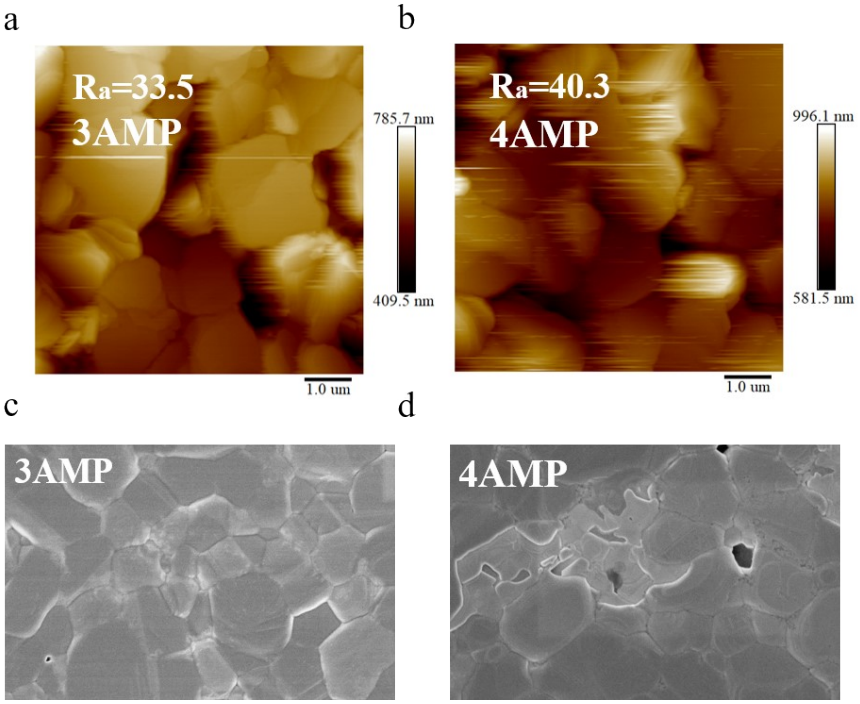

Figure S9

Atomic force microscopy (AFM) images of (a) 3AMP-based perovskite film, (b) 3AMP-based perovskite film.

Scanning electron microscopy (SEM) images of the surface of (c)3AMP-based perovskite film and (d)4AMP-based perovskite film

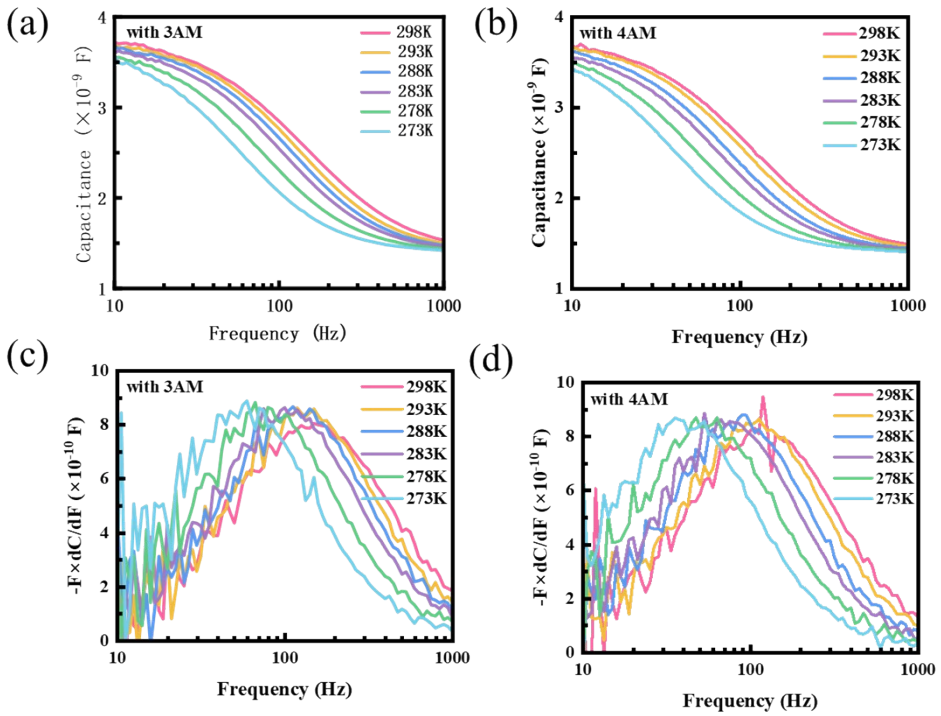

Figure S10.

Capacitance-frequency (C-F) plots of (a) 3AMP-base and (b) 4AMP-base at different temperature. Plots of temperature dependent $-F \times dC/dF$ vs. Frequency for (c) 3AMP-base, (d) 4AMP-base.

Table S1. Fitting parameters of TRPL for control and target perovskite films.

	$\tau_1\ (us)$	$\tau_2\ (\mu s)$	$\tau\ (\mu s)$
3AMP	0.22	2.13	2.04
4AMP	0.15	2.12	1.99

Table S2. Fitting parameters for TAS of bi-exponential decay fits for a series of perovskite films.

	τ1 (ps)	**τ2 (ps)**	**τave (ps)**
3AMP	7.37	512.87	494.11
4AMP	86.58	1243.57	1188.59

Table S3. Summary of photovoltaic parameters of MSPE-treated PSCs. (Hysteresis index (HI) is defined according to the following equation: HI = (PCE_{FS} − PCE_{RS})/PCE_{FS}.)

Sample	Scan direction	V_{OC} (V)	J_{SC} (mA cm^{-2})	FF (%)	PCE (%)	HI[b]
3AMP	Forward	1.153	23.40	75.79	20.45	0.004
	Reverse	1.147	23.53	75.48	20.37	
4AMP	Forward	1.098	22.69	72.42	18.05	0.013
	Reverse	1.103	22.52	73.51	18.28	

References

1 S. Grimme, S. Ehrlich and L. Goerigk, *J Comput Chem*, 2011, **32**, 1456–1465.

2 G. Kresse and J. Furthmüller, *Phys. Rev. B*, 1996, **54**, 11169–11186.

3 J. P. Perdew, K. Burke and M. Ernzerhof, *Phys. Rev. Lett.*, 1996, **77**, 3865–3868.

4 P. E. Blöchl, *Phys. Rev. B*, 1994, **50**, 17953–17979.